Low dissipation spectral filtering using a field-effect tunable III–V hybrid metasurface

Raktim Sarma, Salvatore Campione, Michael Goldflam, Joshua Shank, Jinhyun Noh, Sean Smith, Peide D. Ye, Michael Sinclair, John Klem, Joel Wendt, Isaac Ruiz, Stephen W. Howell, and Igal Brener

Citation: Appl. Phys. Lett. **113**, 061108 (2018); doi: 10.1063/1.5042662
View online: https://doi.org/10.1063/1.5042662
View Table of Contents: http://aip.scitation.org/toc/apl/113/6
Published by the American Institute of Physics

Articles you may be interested in

Effects of modulation p doping in InAs quantum dot lasers on silicon
Applied Physics Letters **113**, 061105 (2018); 10.1063/1.5040792

Active control of polarization-dependent near-field coupling in hybrid metasurfaces
Applied Physics Letters **113**, 061111 (2018); 10.1063/1.5040162

Design of digital coding metasurfaces with independent controls of phase and amplitude responses
Applied Physics Letters **113**, 063502 (2018); 10.1063/1.5043520

An ultra-thin coplanar waveguide filter based on the spoof surface plasmon polaritons
Applied Physics Letters **113**, 071101 (2018); 10.1063/1.5045069

Terahertz metamaterial perfect absorber with continuously tunable air spacer layer
Applied Physics Letters **113**, 061113 (2018); 10.1063/1.5041282

Meta-facet fiber for twisting ultra-broadband light with high phase purity
Applied Physics Letters **113**, 061103 (2018); 10.1063/1.5043268

AIP | Conference Proceedings
Get 30% off all print proceedings!
Enter Promotion Code PDF30 at checkout

APPLIED PHYSICS LETTERS **113**, 061108 (2018)

Low dissipation spectral filtering using a field-effect tunable III–V hybrid metasurface

Raktim Sarma,[1,a)] Salvatore Campione,[1] Michael Goldflam,[1] Joshua Shank,[1] Jinhyun Noh,[2] Sean Smith,[1] Peide D. Ye,[2] Michael Sinclair,[1] John Klem,[1] Joel Wendt,[1] Isaac Ruiz,[1] Stephen W. Howell,[1] and Igal Brener[1,3,a)]

[1]*Sandia National Laboratories, Albuquerque, New Mexico 87185, USA*
[2]*Birck Nanotechnology Center, Purdue University, West Lafayette, Indiana 47907, USA*
[3]*Center for Integrated Nanotechnologies, Sandia National Laboratories, Albuquerque, New Mexico 87185, USA*

(Received 3 June 2018; accepted 23 July 2018; published online 9 August 2018)

Considering the power constrained scaling of silicon complementary metal-oxide-semiconductor technology, the use of high mobility III–V compound semiconductors such as $In_{0.53}Ga_{0.47}As$ in conjunction with high-κ dielectrics is becoming a promising option for future n-type metal-oxide-semiconductor field-effect-transistors. Development of low dissipation field-effect tunable III–V based photonic devices integrated with high-κ dielectrics is therefore very appealing from a technological perspective. In this work, we present an experimental realization of a monolithically integrable, field-effect-tunable, III–V hybrid metasurface operating at long-wave-infrared spectral bands. Our device relies on strong light-matter coupling between epsilon-near-zero (ENZ) modes of an ultra-thin $In_{0.53}Ga_{0.47}As$ layer and the dipole resonances of a complementary plasmonic metasurface. The tuning mechanism of our device is based on field-effect modulation, where we modulate the coupling between the ENZ mode and the metasurface by modifying the carrier density in the ENZ layer using an external bias voltage. Modulating the bias voltage between ± 2 V, we deplete and accumulate carriers in the ENZ layer, which result in spectrally tuning the eigenfrequency of the upper polariton branch at 13 μm by 480 nm and modulating the reflectance by 15%, all with leakage current densities less than 1 $\mu A/cm^2$. Our wavelength scalable approach demonstrates the possibility of designing on-chip voltage-tunable filters compatible with III–V based focal plane arrays at mid- and long-wave-infrared wavelengths. *Published by AIP Publishing.*
https://doi.org/10.1063/1.5042662

With the increasing difficulty of Si to match the complementary metal-oxide-semiconductor (CMOS) scaling given by Moore's law, high-mobility III–V compound semiconductors are being extensively studied as alternative channel materials because of their superior transport properties. Among various III-V semiconductors, $In_{0.53}Ga_{0.47}As$ is rising as a promising option for future n-type MOS field-effect-transistors (MOSFETs).[1] In addition, integration of high-κ dielectrics such as HfO_2 with $In_{0.53}Ga_{0.47}As$ is also being extensively studied to lower leakage currents of devices, which is a fundamental requirement for designing energy efficient low-power integrated electronics.[2] Development of low dissipation field-effect tunable III–V photonic devices integrated with high-κ dielectrics is therefore very appealing as it can create exciting new opportunities for opto-electronic devices.

A prominent on-chip integrable approach for designing tunable optical devices relies on metasurfaces, which are two-dimensional equivalents of bulk metamaterials. With thicknesses less than the wavelength and resonances that can be controlled using the shape and the size of individual resonators, metasurfaces are ideal candidates for building on-chip ultrathin filters. Fabricating a field-effect tunable optical filter using a III–V based metasurface is especially appealing as such a device will be compatible with III–V based devices including focal plane arrays and can provide the functionality of tunable spectral response.

To date, numerous optical, thermal, electromechanical, and voltage-tunable approaches have been employed in the design of tunable metasurfaces.[3–12] In general, voltage-tunable approaches are more appealing as they are easier to integrate with electronics and can be more mechanically robust. Various materials such as graphene, transparent conductive oxides, and liquid crystals have been extensively studied as the active materials for voltage-tunable metasurfaces at visible, near, and mid-infrared wavelengths.[13–21] The *voltage-tunable approaches* based on III–V materials for mid- and long-infrared wavelengths have relied on either depletion-based carrier modulation or Stark effect combined with quantum wells.[22–25] While the previous III–V approaches have demonstrated tuning, they generally had relatively large leakage current densities on the order of A/cm^2.[25] This was primarily because an undoped semiconductor layer was used as a barrier[22–25] instead of a high-κ dielectric. The large modulation of carriers required to observe tuning with previously demonstrated III–V approaches cannot be achieved without large leakage currents; this is because, for a given *semiconductor barrier*, the leakage currents increase rapidly with reverse bias.[23]

In this work, we demonstrate a III–V hybrid tunable metasurface which uses n-doped $In_{0.53}Ga_{0.47}As$ as the active material and HfO_2 as the gate dielectric. Our device employs field-effect tuning which allows us to modulate the optical

[a)]Authors to whom correspondence should be addressed: rsarma@sandia.gov and ibrener@sandia.gov

response of the metasurface with negligible leakage currents, thereby making it a low dissipation device and therefore energy efficient. By depleting or accumulating carriers in the active $In_{0.53}Ga_{0.47}As$ layer, we can create a large modulation in the optical response of the metasurface, still with negligible leakage current. Compared to the most recent and efficient III–V approach,[25] our device exhibits six orders of magnitude lower leakage current and demonstrates significantly larger spectral tuning with much lower bias voltage. Our hybrid device fulfils the low size, low weight, and low power (SWaP) criteria and is fully compatible with current nanofabrication processes of $In_{0.53}Ga_{0.47}As$-based electronic devices. Finally, although demonstrated here for long-infrared wavelengths, our approach is scalable to other wavelength ranges (e.g., mid-infrared); it represents significant progress in the emerging area of III–V photonics and fulfills the emerging need for tunable photonic devices in the mid- and long-infrared wavelengths for sensing and thermal imaging applications.

The tunable metasurface presented in Fig. 1(a) is based on a principle demonstrated previously in different semiconductor systems.[22,26,27] The device relies on strong coupling between the dipole resonances supported by a complementary plasmonic metasurface and epsilon-near-zero (ENZ) modes supported in an ultrathin $In_{0.53}Ga_{0.47}As$ layer. The ENZ modes are plasmon modes occurring at the plasma frequency of an extremely thin layer of Drude material such as highly doped semiconductor.[26,28–30] The ENZ modes require electric field components normal to the layers for excitation. Since the dipole resonances of the metasurface can generate normal field components in the near field, by exciting the resonances of the metasurface we can also excite the ENZ modes supported in an ultrathin semiconductor layer underneath the metasurface. The excitation of the ENZ modes by the resonators can lead to strong polaritonic coupling where periodic exchange of energy occurs between the two resonant systems and that can be observed in the spectral domain as a frequency splitting (Rabi splitting) with respect to the resonant frequency of the uncoupled metasurface. Because the polaritonic coupling can be modulated by controlling the carrier density in the semiconductor layer, which in turn will modify the spectral response of the coupled system, this principle provides a voltage-tunable approach to design a tunable metasurface.

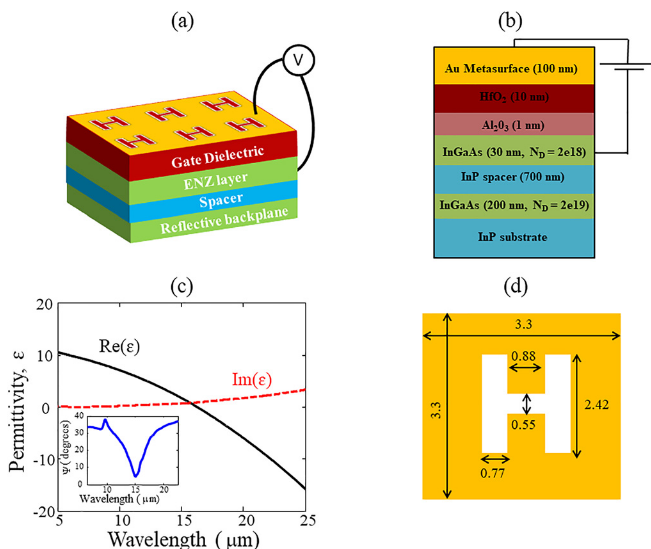

FIG. 1. (a) Three-dimensional schematic of the metasurface-semiconductor coupled structure. (b) The stack of different layers that were grown to fabricate the device. (c) Real and imaginary parts of the permittivity of doped $In_{0.53}Ga_{0.47}As$ ($N_D = 2 \times 10^{18}\,cm^{-3}$). The inset shows the experimental measurement of the ellipsometric angle ψ as a function of wavelength of the bare wafer without any resonators to show the Berreman feature (a dip at $\sim 15\,\mu m$) associated with the ENZ crossing. The second smaller dip at $\sim 10\,\mu m$ can be attributed to the Berreman feature of the 200 nm $In_{0.53}Ga_{0.47}As$ layer with a higher doping density of $N_D = 2 \times 10^{19}\,cm^{-3}$. (d) Dimensions of the dogbone complementary resonator (scale factor 1.0) in micrometers optimized using finite-difference-time domain simulations.

To optimize the performance of our hybrid device, we carefully designed each component of the metasurface-semiconductor coupled system. Figure 1(b) shows the cross-section of the semiconductor layers that were grown using molecular beam epitaxy on an InP substrate. The epitaxial layers were lattice matched to reduce strain induced defects and enhance mobility. As compared to group IV semiconductors and III-V semiconductors such as GaAs, using $In_{0.53}Ga_{0.47}As$ as the active ENZ material has an additional advantage of having a low effective electron mass of $0.024m_0$. Since ENZ modes exist at the plasma frequency, a low effective electron mass allows us to reduce the doping requirement for a given plasma frequency. Because of the inverse relationship between the electron depletion width and the doping density, a lower doping density creates the opportunity for larger modulation of carrier density by depletion. In this device, we chose a doping density of $N_D = 2 \times 10^{18}\,cm^{-3}$ for the 30 nm $In_{0.53}Ga_{0.47}As$ ENZ layer which results in a plasma frequency of $\sim 15.5\,\mu m$ [Fig. 1(c)]. We confirmed the ENZ spectral position experimentally by performing ellipsometry measurements of the bare wafer, which resulted into the so-called "Berreman dip" feature [see the inset of Fig. 1(c)].[26,29]

For efficient voltage-controlled modulation of carrier density, it is crucial to have a low defect interface between the ENZ layer and the gate dielectric. Interfaces with defects lead to Fermi level pinning and reduce the ability to deplete electrons from the active semiconductor layer. A platform based on $In_{0.53}Ga_{0.47}As$ as the ENZ material gives us an advantage of using HfO_2 as the high-κ gate dielectric as the $HfO_2/In_{0.53}Ga_{0.47}As$ interface has been extensively characterized for high mobility MOSFET applications.[2] In addition, HfO_2 is optically transparent at the wavelengths of interest. It has been shown that to generate a high quality $HfO_2/In_{0.53}Ga_{0.47}As$ interface, insertion of an ultrathin layer of Al_2O_3 between the HfO_2 and $In_{0.53}Ga_{0.47}As$ layers is beneficial as it improves the interface properties, reduces interface trap density, and lowers leakage currents.[2] We therefore used atomic layer deposition (ALD) to deposit HfO_2 with an Al_2O_3 interlayer for our gate dielectric. In addition, prior to ALD deposition, we performed surface cleaning procedures using buffer oxide etch to remove native oxides and performed surface passivation using $(NH_4)_2S$ to improve the interface properties and reduce interface trap density.[31]

The complementary design for our metasurface offers a continuous gold layer that can be used as a top contact for voltage tuning and it ensures the homogeneous distribution of the applied voltage along the lateral directions across the

entire array of resonators. We chose the "dogbone" resonator [Fig. 1(d)] shape as it has high capacitance compared to conventional shapes such as circular split-ring resonators,[32] which leads to more efficient light-matter coupling resulting in larger Rabi splitting.[32] In addition, the dogbone resonator has strong near-field enhancement along the entire area of the resonator. To capture the effect of the two-dimensional array (similar to the fabricated samples), we performed finite-difference time-domain (FDTD) simulations[33] of a single unit cell with periodic boundary conditions using permittivities extracted from ellipsometric measurements. These simulations allowed us to determine the dimensions of the resonator such that the metasurface resonance is spectrally close to the ENZ resonance frequency to ensure polaritonic coupling. Figure 1(d) shows the dimensions of scale factor 1.0 of the dogbone resonator with a resonant wavelength of $\sim 14.5\,\mu$m [when the scaling factor is varied, all marked dimensions in Fig. 1(d) are scaled accordingly]. Finally, since the device is designed to work in the reflection mode, we added a 200 nm highly doped $In_{0.53}Ga_{0.47}As$ layer ($N_D = 2 \times 10^{19}\,cm^{-3}$) underneath the ENZ layer: its plasma frequency is at $\sim 10\,\mu$m [Fig. 1(c) inset]; thus, this highly doped layer acts as a metallic backplane for all the longer wavelengths which are of interest to us. The reflecting backplane prevents the optical fields of the resonator from penetrating into the substrate and leads to larger mode confinement.[34]

Figure 2(a) shows scanning electron micrographs of the fabricated metasurface. The complementary dogbone resonators were defined using electron-beam lithography. Such process was followed by evaporation of Ti/Au (5 nm/100 nm) and a lift-off process. For electrical biasing, we defined mesas by wet-chemical etching. The bottom contact was processed as the Ti/Au/Ag/Au ohmic contact directly on top of the ENZ layer. We fabricated resonators with different geometric scale factors on top of the same heterostructure, which exhibits different bare cavity resonant frequencies, to confirm experimentally (without applying any bias) the anti-crossing behavior of the two polariton branches due to strong light-matter interaction. Room temperature reflectance measurements of these devices using a FTIR spectrometer with a microscope objective of NA = 0.4 are shown in Fig. 2(b). All the measurements were referenced against an unpatterned gold region which allowed us to remove the spectral dependency of the spectrometer and capture only the metasurface response. As expected, a clear anti-crossing is observed which confirms polaritonic coupling between the dipole resonances of the metasurface and the ENZ modes.

Next, we performed electrical characterization of our fabricated devices to monitor the leakage currents and confirm modulation of the carrier density of the ENZ layer upon application of a bias. Figure 3(a) shows current densities as a function of applied bias. For voltages within the range of ± 2 V, we see leakage current densities smaller than 1 μA/cm^2. As shown in Fig. 3(b), for the same range of voltages, we observe a change in the capacitance of the device which indicates modulation of the carrier density in the ENZ layer. A negative voltage on the metasurface leads to depletion of carriers in the ENZ layer, while a positive voltage on the metasurface leads to accumulation of carriers. Figure 3(c) shows a schematic of three different carrier density distributions of the ENZ layer for three different cases of voltage bias. We performed high frequency capacitance-voltage measurements and the depletion width in the ENZ layer was measured to be ~ 10 nm. There is no direct way to measure the carrier density distribution and the width of the accumulation layer using capacitance-voltage measurements and such a study is beyond the scope of this work.

Finally, we performed the voltage tuning experiment where we investigated the optical response of a metasurface with resonators of scale factor 0.9 as a function of voltage bias. Figure 4(a) shows room temperature FTIR reflectance

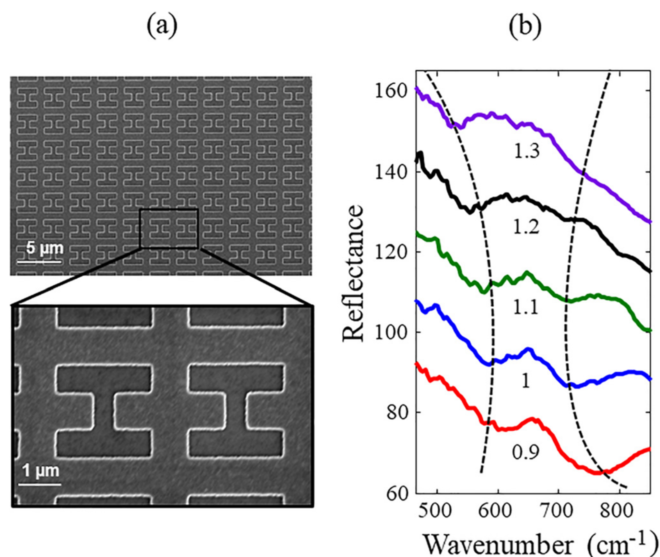

FIG. 2. (a) Scanning electron micrographs of a fabricated metasurface with resonators of scale factor 1.0. (b) Room temperature FTIR reflectance measurements of metasurfaces with series of resonators with different geometric scale factors (from 0.9 to 1.3 with step of 0.1). For clarity, the reflectance curves are offset from each other vertically by 20%. The two dips in the reflection spectrum correspond to the two polariton branches and clear anti-crossing behavior of the splitting between the two polariton branches is observed. The dashed lines representing the two polariton branches are shown as guides to the eye.

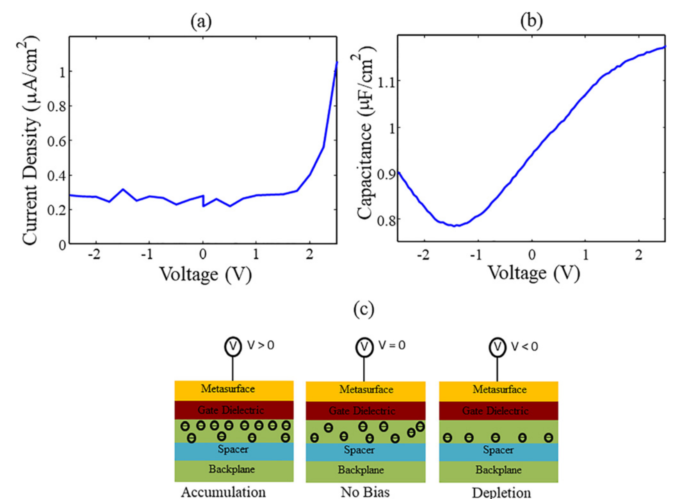

FIG. 3. (a) Static current-voltage characteristics of the device. (b) Capacitance-voltage measurements at the frequency of 1 kHz. (c) Schematic showing the carrier density distribution in the ENZ layer (green layer between the gate dielectric and the spacer layer) for 3 different bias conditions: (left) accumulation, (center) no bias, and (right) depletion.

measurements for three different bias-voltages, namely ± 2 V and 0 V. We see a clear spectral tuning and amplitude modulation of reflectance for the three cases. The change in the reflectance spectrum can be understood as follows: depletion leads to reduction of the effective thickness of the ENZ layer and this leads to the reduction of the polaritonic splitting due to weaker light-matter interaction. The two polariton branches therefore become spectrally closer to each other compared to an unbiased case. Accumulation, on the other hand, leads to an increase in the carrier density in the ENZ layer, which leads to an increase in its plasma frequency. This leads to a decrease in the real part of the dielectric permittivity of the ENZ layer. In this case, since the scale factor of the resonator is such that we are not exactly at the anti-crossing point [see Fig. 2(b)], the upper polariton branch at $\lambda_1 \sim 13\,\mu$m is more "resonator-like" and the lower polariton branch at $\lambda_2 \sim 16\,\mu$m is more "matter-like". The change in permittivity of the ENZ layer therefore leads to blue shifting of the eigenfrequency of the upper polariton branch. The spectral tuning is less prominent for the lower polariton branch as it is more "matter-like" and the effect of charge modulation instead is more apparent in the form of amplitude modulation of the reflectance.

Figure 4(b) shows FDTD simulations of the three experimental cases for qualitative comparison to the experiment. In the case of depletion, the simulation assumes a depletion width of 10 nm completely void of carriers. For accumulation, the simulation assumes an accumulation layer of 1 nm with increased carrier density of 1×10^{19} cm^{-3}. A good qualitative comparison between the experiment and simulations is

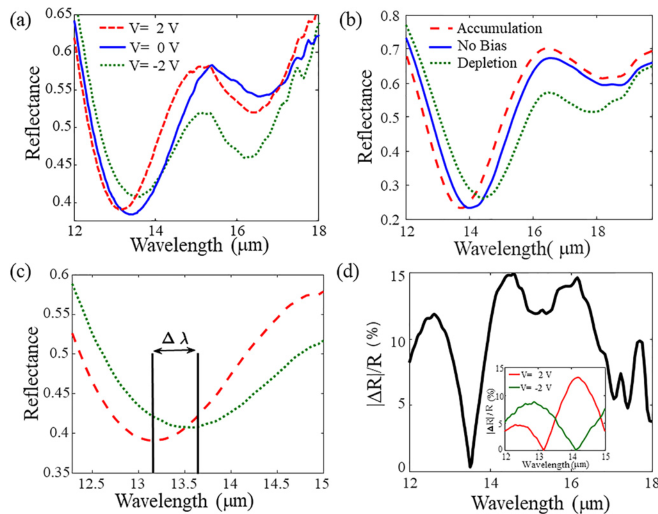

FIG. 4. (a) Room temperature reflectance measurement of a metasurface with resonators of scale factor 0.9 for 3 different bias conditions (V = 0 V (blue solid), +2 V (red dashed) and −2 V (green dotted)). (b) FDTD simulation results of reflectance of a metasurface with resonators of scale factor 0.9 for 3 different conditions of no bias (blue solid), accumulation (red dashed) and depletion (green dotted). (c) A zoomed plot of experimentally measured reflectance spectrum of the upper polariton branch for the two conditions of accumulation (V = +2 V, red dashed line), and depletion (V = −2 V, green dotted line). A clear spectral tuning, $\Delta\lambda = 480$ nm, of the dip in the reflection spectrum is observed. (d) Experimental data for the relative change in reflectance, $|\Delta R|/R = |(R_{V=2V.} - R_{V=-2V.})|/R_{V=-2V}$ for the conditions of depletion (V = −2 V) and accumulation (V = +2 V). The inset shows the relative change in reflectance, $|\Delta R|/R = |(R_{V=\pm 2V} - R_{V=0})|/R_{V=0}$ for depletion (V = −2 V, green line) and accumulation (V = +2 V, red line) with respect to reflectance with no bias (V = 0 V).

observed. It is important to note here that a direct quantitative comparison between the experiment and simulations cannot be made for three main reasons. First, in real experiments for the case of depletion, the depletion width is not completely void of carriers as assumed in the simulation. The depletion width usually has a spatially varying distribution of carriers. Second, since it is not straightforward to determine the exact width and the carrier density distribution of the accumulation layer, the parameters used in the simulation for accumulation are approximations and third, the simulations were performed for plane waves at normal incidence whereas in the experiment there is a large spread of incoming angles due to the use of an objective with NA = 0.4. Nevertheless, we see very good qualitative agreement between the experimental results and the numerical simulations which confirms spectral tuning and amplitude modulation of reflectance due to modulation of polaritonic coupling between the ENZ modes and the metasurface resonances on application of voltage bias.

To quantify the experimentally observed voltage-controlled spectral tuning and amplitude modulation, we looked at the change in eigenfrequencies (corresponding to the minimum/dip in the reflection spectrum) of the upper polariton branch and the relative change in the amplitude of the reflectance of both the polariton branches [Figs. 4(c) and 4(d)]. The eigenfrequency of the upper polariton branch, which is 13.4 μm for no bias, gets blue-shifted to 13.13 μm under accumulation and red-shifted to 13.61 μm under depletion [Fig. 4(c)]. We therefore observed experimentally a spectral tuning $\Delta\lambda$ of 480 nm by accumulating and depleting the carriers in the ENZ layer. In addition, as shown in Fig. 4(d), we also observe a significant relative change in magnitude of the reflectance, $|\Delta R|/R = |(R_{V=2V.} - R_{V=-2V.})|/R_{V=-2V}$. The relative change in reflectance varies spectrally and can be as large as 15%.

In conclusion, we demonstrated experimentally a monolithically integrable, low dissipation, field-effect tunable III–V based hybrid metasurface operating at long-wave-infrared spectral bands. Our device works in the regime of strong light-matter interaction and relies on the principle of modulating the coupling between the ENZ modes in an ultrathin semiconductor layer and the metasurface by modifying the carrier density in the ENZ layer using an external bias. Although demonstrated for long-wave-infrared wavelengths, the operating wavelength of our device can be scaled to other ranges such as mid-infrared as the primary factor determining it is the plasma frequency of the ENZ layer and that can be varied by varying the doping density. In our future studies, we plan to investigate different metasurface designs with resonances with higher quality factors and therefore narrower spectral widths. On applying a bias, such designs may enable us to spectrally tune the resonator-like polariton branch by more than its linewidth, which will enable us to observe larger voltage-induced reflectance modulation.

This work was performed, in part, at the Center for Integrated Nanotechnologies, an Office of Science User Facility operated for the U.S. Department of Energy (DOE) Office of Science. It was also partially supported by the Laboratory Directed Research and Development program at

Sandia National Laboratories. Sandia National Laboratories is a multi-mission laboratory managed and operated by National Technology and Engineering Solutions of Sandia, LLC, a wholly owned subsidiary of Honeywell International, Inc., for the U.S. Department of Energy's National Nuclear Security Administration under Contract No. DE-NA0003525. This paper describes the objective technical results and analysis. Any subjective views or opinions that might be expressed in the paper do not necessarily represent the views of the U.S. Department of Energy or the United States Government.

[1]J. A. del Alamo, D. A. Antoniadis, J. Lin, W. Lu, A. Vardi, and X. Zhao, in *Compound Semiconductor Integrated Circuit Symposium (CSICS)*, New Orleans, USA, 11–14 October 2015, pp. 1–4.
[2]R. Suzuki, N. Taoka, M. Yokoyama, S. Lee, S. H. Kim, T. Hoshii, T. Yasuda, W. Jevasuwan, T. Maeda, O. Ichikawa, N. Fukuhara, M. Hata, M. Takenaka, and S. Takagi, Appl. Phys. Lett. **100**, 132906 (2012).
[3]J. M. Manceau, N. H. Shen, M. Kafesaki, C. M. Soukoulis, and S. Tzortzakis, Appl. Phys. Lett. **96**, 021111 (2010).
[4]R. Singh, A. K. Azad, Q. X. Jia, A. J. Taylor, and H. T. Chen, Opt. Lett. **36**, 1230 (2011).
[5]P. P. Iyer, M. Pendharkar, C. J. Palmstrom, and J. A. Schuller, Nat. Commun. **8**, 472 (2017).
[6]M. J. Dicken, K. Aydin, I. M. Pryce, L. A. Sweatlock, E. M. Boyd, S. Walavalkar, J. Ma, and H. A. Atwater, Opt. Express **17**, 18330 (2009).
[7]A. Kundu, S. Das, S. Maity, B. Gupta, S. K. Lahiri, and H. Saha, J. Micromech. Microeng. **22**, 045004 (2012).
[8]X. Zhao, J. Schalch, J. Zhang, H. R. Seren, G. Duan, R. D. Averitt, and X. Zhang, Optica **5**, 303 (2018).
[9]E. Arbabi, A. Arbabi, S. M. Kamali, Y. Horie, M. Faraji-Dana, and A. Faraon, Nat. Commun. **9**, 812 (2018).
[10]Q. Zhao, L. Kang, B. Du, B. Li, J. Zhou, H. Tang, X. Liang, and B. Zhang, Appl. Phys. Lett. **90**, 011112 (2007).
[11]M. Decker, C. Kremers, A. Minovich, I. Staude, A. E. Miroshnichenko, D. Chigrin, D. N. Neshev, C. Jagadish, and Y. S. Kivshar, Opt. Express **21**, 8879 (2013).
[12]A. Komar, Z. Fang, J. Bohn, J. Sautter, M. Decker, A. Miroshnichenko, T. Pertsch, I. Brener, Y. S. Kivshar, I. Staude, and D. N. Neshev, Appl. Phys. Lett. **110**, 071109 (2017).
[13]L. Ju, B. Geng, J. Horng, C. Girit, M. Martin, Z. Hao, H. A. Bechtel, X. Liang, A. Zettl, Y. R. Shen, and F. Wang, Nat. Nanotechnol. **6**, 630 (2011).
[14]N. K. Emani, T. F. Chung, A. V. Kildishev, V. M. Shalaev, Y. P. Chen, and A. Boltasseva, Nano Lett. **14**, 78 (2014).
[15]M. C. Sherrott, P. W. C. Hon, K. T. Fountaine, J. C. Garcia, S. M. Ponti, S. M. Ponti, V. W. Brar, L. A. Sweatlock, and H. A. Atwater, Nano Lett. **17**, 3027 (2017).
[16]N. Dabidian, I. Kholmanov, A. B. Khanikaev, K. Tatar, S. Trendafilov, S. H. Mousavi, C. Magnuson, R. S. Ruoff, and G. Shvets, ACS Photonics **2**, 216 (2015).
[17]Y. Yao, R. Shankar, M. A. Kats, Y. Song, J. Kong, M. Loncar, and F. Capasso, Nano Lett. **14**, 6526 (2014).
[18]Y. W. Huang, H. H. Lee, R. Sokhoyan, R. A. Pala, K. Thyagarajan, S. Han, D. P. Tsai, and H. A. Atwater, Nano Lett. **16**, 5319 (2016).
[19]J. Park, J. H. Kang, X. Liu, and M. L. Brongersma, Sci. Rep. **5**, 15754 (2015).
[20]J. Park, J. H. Kang, S. J. Kim, X. Liu, and M. L. Brongersma, Nano Lett. **17**, 407 (2017).
[21]A. Komar, R. Paniagua-Dominguez, A. Miroshnichenko, Y. Yu, Y. S. Kivshar, A. I. Kuznetsov, and D. Neshev, ACS Photonics **5**, 1742 (2018).
[22]Y. C. Jun, J. Reno, T. Ribaudo, E. Shaner, J. J. Greffet, S. Vassant, F. Marquier, M. Sinclair, and I. Brener, Nano Lett. **13**, 5391 (2013).
[23]Y. C. Jun and I. Brener, J. Opt. **14**, 114013 (2012).
[24]A. Benz, I. Montano, J. F. Klem, and I. Brener, Appl. Phys. Lett. **103**, 263116 (2013).
[25]J. Lee, S. Jung, P. Y. Chen, F. Lu, F. Demmerle, G. Boehm, M. C. Amann, A. Alu, and M. A. Belkin, Adv. Opt. Mater. **2**(11), 1057 (2014).
[26]O. Wolf, S. Campione, J. Kim, and I. Brener, Opt. Express **24**, 21512 (2016).
[27]S. Campione, S. Liu, A. Benz, J. F. Klem, M. B. Sinclair, and I. Brener, Phys. Rev. Appl. **4**, 044011 (2015).
[28]S. Campione, I. Brener, and F. Marquier, Phys. Rev. B **91**, 121408(R) (2015).
[29]S. Vassant, J. P. Hugonin, F. Marquier, and J. J. Greffet, Opt. Express **20**, 23971 (2012).
[30]S. Campione, I. Kim, D. de Ceglia, G. A. Keeler, and T. S. Luk, Opt. Express **24**, 18782 (2016).
[31]J. F. Fan, H. Oigawa, and Y. Nannichi, Jpn. J. Appl. Phys., Part 2 **27**, L1331 (1988).
[32]A. Benz, S. Campione, J. F. Klem, M. B. Sinclair, and I. Brener, Nano Lett. **15**, 1959 (2015).
[33]FDTD Lumerical Inc., https://www.lumerical.com/ for "FDTD Solutions."
[34]A. Benz, S. Campione, S. Liu, I. Montano, J. F. Klem, M. Sinclair, F. Capolino, and I. Brener, Opt. Express **21**, 32572 (2013).